A geometrical approach to Feenberg multiple-scattering series

1998 J. Phys. A: Math. Gen. 31 2837

(http://iopscience.iop.org/0305-4470/31/12/009)

J. Phys. A: Math. Gen. **31** (1998) 2837–2852. Printed in the UK PII: S0305-4470(98)84409-0

A geometrical approach to Feenberg multiple-scattering series

Subhradip Ghosh, Nityananda Das and A Mookerjee

S N Bose National Centre for Basic Sciences, J D Block, Sector 3, Salt Lake City, Calcutta 700091, India

Received 20 May 1997, in final form 14 November 1997

Abstract. We present here a graphical approach to the Feenberg multiple-scattering expansion and discuss examples of Hamiltonians with topological and substitutional disorder where the path-contribution technique allows us to understand the effects of such disorder and generate physically relevant approximations.

1. Introduction

The Feenberg renormalized perturbation forms one of the bedrocks of multiple-scattering theory. The original formal proof offered by Feenberg was based on algebraic resummation. We offer here an alternative justification based on the idea of path summations. The geometric interpretation of such scattering terms was first proposed by Haydock [1] and although a similar geometrical interpretation was used in several communications on disordered systems [2], the striking beauty and simplicity of the method has not been explored in the way it should have been. The visualization of contributions from walks on a lattice is perhaps more immediately comprehensible than intricate algebraic resummations. We shall use the ideas developed here to study how structures form in the density of states. In particular, when the system contains either spatial or topological disorder and the usual band-structure methods for crystals become inapplicable, the path-contribution technique gives us an insight into the origin of structures in the density of states and helps us in developing physically relevant approximations. We shall provide several examples of the above.

2. Multiple-scattering theory

2.1. The Feenberg series

We shall choose a countable, orthogonal basis set $\{|i\rangle\}$. It is enough that the basis is countable. The index i is in general a composite index for an electron in a solid. For example, it could denote $\{R, r_\alpha, \ell, m, m_s\}$, where R labels a particular unit cell, r_α is the position of a particular member of the basis within that cell and the remaining labels are the usual spherical harmonic and spin quantum numbers. With respect to this basis the Hamiltonian may be represented by the operator

$$\boldsymbol{H} = \sum_i \epsilon_i |i\rangle\langle i| + \sum_i \sum_{j\neq i} t_{ij} |i\rangle\langle j| = \boldsymbol{H}_0 + \boldsymbol{H}_1. \tag{1}$$

0305-4470/98/122837+16$19.50

The break-up of the Hamiltonian into an unscattered term $\boldsymbol{H}_0$ and a scattering term $\boldsymbol{H}_1$ is not unique. It is our choice how we decide to partition the Hamiltonian. Usually our choice of $\boldsymbol{H}_0$ is the one for which the unperturbed resolvent $\boldsymbol{g}(z) = (z\boldsymbol{I} - \boldsymbol{H}_0)^{-1}$ is relatively easy to obtain exactly. For the above choice, since $\boldsymbol{H}_0$ is totally diagonal:

$$\boldsymbol{g}(z) = \frac{1}{z - \epsilon_i}\boldsymbol{I}.$$

Now, simple matrix algebra gives,

$$\boldsymbol{G}(z) = \boldsymbol{g} + \boldsymbol{g}\boldsymbol{H}_1\boldsymbol{g} + \boldsymbol{g}\boldsymbol{H}_1\boldsymbol{g}\boldsymbol{H}_1\boldsymbol{g} + \cdots \tag{2}$$

This is the bare multiple-scattering series. The diagonal representation in the countable basis gives,

$$G_{ii} = g_{ii} + \sum_{j\neq i} g_{ii}t_{ij}g_{jj}t_{ji}g_{ii} + \cdots + \sum_{j\neq i}\sum_{k\neq j}\cdots\sum_{m\neq n} g_{ii}t_{ij}g_{jj}t_{jk}g_{kk}\ldots t_{mi}g_{ii} + \cdots. \tag{3}$$

2.2. Graphical translation

With each member of the basis $|i\rangle$ we now associate a *vertex* v_i. The set of vertices constitute a *network*. A connection between two vertices v_i and v_j is called a *link* ℓ_{ij}. In case that the index simply refers to a cell R, the network is identical to the underlying lattice made up of these unit cells. For the more general case the network is fully defined by the geometrical connections between its vertices via its links.

Let us now define graphical terminology.

(i) A *path* is defined to be a sequence of vertices connected by links. The number of links is defined to be the *length* of a path. A path of length N between the vertices v_i and v_j is denoted by

$$P_{ij}^N = \{v_i, \ell_{ii}, V_{i_1}, \ell_{i_1i_2}, v_{i_2}\ldots\ell_{i_{N-1}j}, v_j\}.$$

(ii) A closed path is a path whose starting and ending vertices are the same, e.g. P_{ii}^N.

(iii) Vertices which are neither the starting nor the ending vertices on a path are called the *internal vertices*.

(iv) A *closed loose ended* path is defined as the sequence defining a closed path minus the starting (ending) vertex. A closed loose ended path of length N will be denoted by $Q_{ii}^N = \{\ell_{ii_1}, v_{i_1}, \ell_{i_1i_2}, v_{i_2}, \ldots\ell_{i_{N-1}j}\}$.

(v) A closed loose ended path from v_i to v_i which does not visit v_i again, i.e. none of whose internal vertices is v_i will be denoted by S_{ii}^N.

(vi) The *set* of all paths of a particular kind will be denoted by the corresponding curly letter. For example, the set of all closed paths of length N from v_i back to v_i will be denoted by $\mathcal{P}_{ii}^N$.

(vii) The *product* of two paths $P_{ij}^N = \{v_i\ell_{ii_1}v_{i_1}\ldots v_j\}$ and $P_{jk}^M = \{v_j\ell_{jj_1}\ldots v_k\}$ is just another path composed of these two: $P_{ik}^{N+M} = \{v_i\ell_{ii_1}v_{i_1}\ldots v_j\ell_{jj_1}v_{j_1}\ldots v_k\}$.

Note that since paths are *sequences*, this definition of product is not commutative. Moreover, two paths are product compatible only if the endpoint of the first coincides with the starting point of the second. We shall denote the product by $P_{ij}^N \times P_{jk}^M = P_{ik}^{N+M}$.

(viii) The product of two sets of paths $\mathcal{P}_{ij}^N$ and $\mathcal{P}_{jk}^M$ is the set of all possible products of one path from the first set with one from the second. We denote this by : $\mathcal{P}_{ij}^N \odot \mathcal{P}_{jk}^M = \mathcal{P}_{ik}^{N+M}$.

(ix) Any path can be written as a product of its vertices, which are considered paths of length zero, $P_{ii}^0 = v_i$ and its links, which are considered as paths of length one, $P_{ij}^1 = \ell_{ij}$. For example, taking the path described above : $P_{ij}^N = P_{ii}^0 \times P_{ii_1}^1 \times P_{i_1}^0 \times \ldots P_{jj}^0$.

(ix) $\mathcal{P}_{ii}^0 = \{v_i\}$ and $\mathcal{P}_{ii}^N = \mathcal{P}_{ii}^0 \odot \mathcal{Q}_{ii}^N \odot \mathcal{P}_{ii}^0$.

We may now introduce algebraic structure on these abstract graphical objects.

(i) The *contribution* of a vertex v_i is defined to be $\kappa(v_i) = g_{ii}$. The contribution of a link ℓ_{ij} is defined as $\kappa(\ell_{ij}) = t_{ij}$.

(ii) The contribution of a product of objects is defined to the *simple product* of their contributions. Since a path can be written as an ordered product of its vertices and links, it follows that the contribution of a path is a product of the contributions of its vertices and links.

$$\kappa(P_{ij}^N) = \prod_k \kappa(v_k) \prod_{ij} \kappa(\ell_{ij}).$$

(iii) The contribution of a set of paths is the *sum* of contributions of each path in the set.

$$\kappa(\mathcal{P}_{ij}^N) = \sum_{P_{ij}^N \in \mathcal{P}_{ij}^N} \kappa(P_{ii}^N).$$

(iv) The contribution of the *union* of two sets of paths is the sum of the contributions of each set.

$$\kappa(\mathcal{P}_{ij}^N \cup \mathcal{P}_{mn}^M) = \kappa(\mathcal{P}_{ij}^N) + \kappa(\mathcal{P}_{mn}^M).$$

(v) The contribution of the *product* of two sets of paths is the product of the contribution of each set of paths.

Having defined the algebra of paths, let us return our attention to equation (3). If we can define $\mathcal{P}_{ii}^N$ as the set of all closed paths from the vertex v_i and back, and define $\mathcal{P}_{ii}$ as the union of all such paths of all lengths from 1 to ∞:

$$\mathcal{P}_{ii} = \cup_{N=1}^{\infty} \mathcal{P}_{ii}^n$$

then the Feenberg perturbation series can be written in a simple form

$$G_{ii}(z) = \kappa(\mathcal{P}_{ii}^0) + \kappa(\mathcal{P}_{ii}). \tag{4}$$

2.3. Decorations and self energy

Let us now closely examine various paths in the Feenberg series. They are all closed paths. The first thing we do is to rewrite closed paths as a product of vertices and closed loose ended paths $P_{ii}^N = v_i \times Q_{ii}^N \times v_i$.

If we look at figure 1†we notice that all loose ended paths Q_{ii}^N may visit the starting (ending) vertices v_i at most $= N$ (mod) 2 times more. If p denotes the number of times which a closed path visits the starting vertex, then figure 1 shows different paths with different labelling by N and p. Note that

$$\begin{aligned} Q_{ii}^N &= \{\ell_{ii_1} V_{i_i} \ldots \ell_{i_{m_1} i}\} v_i \{\ell_{i i_{m_1+1}} v_{i_{m_1+1}} \ldots \ell_{i_{m_1+m_2-1} i}\} v_i \ldots \\ &= s_{ii}^{m_1} \times P_{ii}^0 \times S_{ii}^{m_2} \times P_{ii}^0 \times \ldots S_{ii}^{m_p} \\ &= Q_{ii}^{p,N}. \end{aligned}$$

† In figures 1–4 which illustrate various walks on the lattice, an arrow $\rightarrow$ or $\leftarrow$ refers to the direction of the walk on the lattice. A bond with two arrows $\rightarrow\leftarrow$ refers to a part of the walk from the vertex at one end of the bond to the other and back. The starting vertex of the walk is also clearly marked.

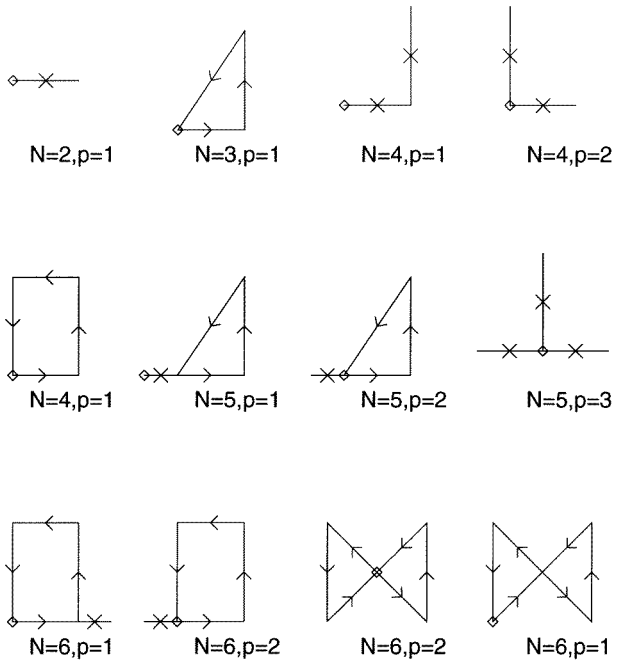

Figure 1. Closed paths labelled by their lengths N and the number of times p it visits the initial vertex internally.

Looking at the bottom of the figure 1 we see that,

$$Q_{ii}^{1,6} = S_{ii}^{6}$$
$$Q_{ii}^{2,6} = S_{ii}^{2} \times P_{ii}^{0} \times S_{ii}^{4}$$
$$Q_{ii}^{2,6} = S_{ii}^{3} \times P_{ii}^{0} \times S_{ii}^{3}$$
$$Q_{ii}^{1,6} = S_{ii}^{6}.$$

The network produced by the unscattering Hamiltonian $\boldsymbol{H}_0$ is just a set of unlinked vertices, since $\boldsymbol{H}_0$ is totally diagonal. We note from figure 1 that the closed loose ended paths $Q_{ii}^{p,N}$ decorate or hang onto the vertices of that network. These decorations arise entirely because of the scattering due to $\boldsymbol{H}_1$. They are therefore *central* to our study.

If we now group together all loose ended closed paths with the same value of p and call

$$\hat{\mathcal{Q}}_{ii}^{p} = \cup_{N=2^p}^{\infty} \mathcal{Q}_{ii}^{p,N}.$$

Comparing figures 1 and 2 we see that this regrouping takes care of all closed loose ended paths starting and ending at the vertex v_i.

$$\mathcal{Q}_{ii} = \cup_{p=1}^{\infty} \cup_{N=2^p}^{\infty} \mathcal{Q}_{ii}^{p,N} = \cup_{m=0}^{\infty} \hat{\mathcal{Q}}_{ii}^{p}.$$

If we now examine the paths in figure 2 a little more carefully, we denote that any path in the second row with $p = 2$ can be broken up into two paths from the top row with $p = 1$. Similarly, any path with $p = 3$ in the bottom row can be broken up into three paths from the top row with $p = 1$. The break-up structure is now evident:

$$\hat{\mathcal{Q}}_{ii}^{p} = \hat{\mathcal{Q}}_{ii}^{1} \odot \mathcal{P}_{ii}^{1} \odot \hat{\mathcal{Q}}_{ii}^{1} \ldots \odot \hat{\mathcal{Q}}_{ii}^{1} (p-1) \text{ times}.$$

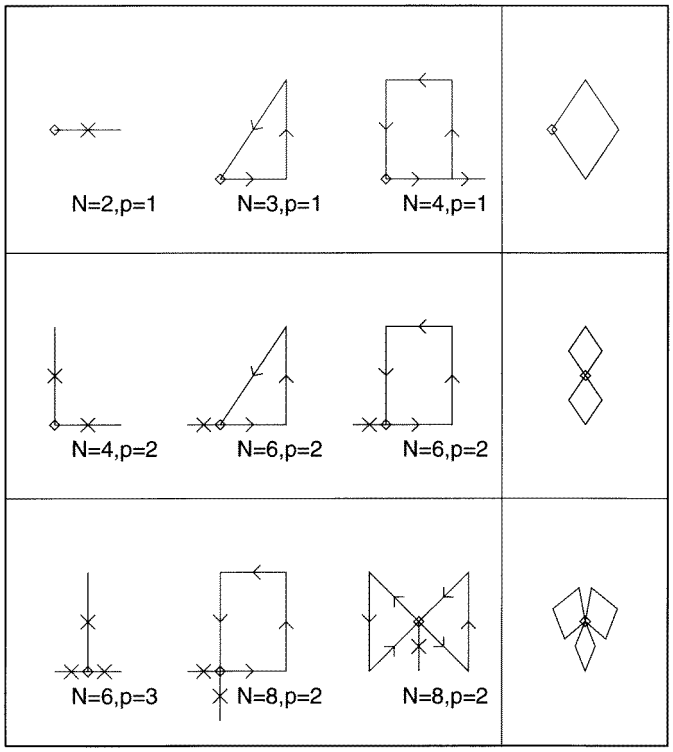

Figure 2. Grouping of closed paths with the same value of p to produce decorations of the internal vertex.

It then follows from the above equation that,

$$\mathcal{Q}_{ii} = \cup_{p=1}^{\infty} \hat{\mathcal{Q}}_{ii}^{1} \odot (\mathcal{P}_{ii}^{0} \odot \hat{\mathcal{Q}}_{ii}^{1})^{p-1}. \tag{5}$$

So that,

$$\begin{aligned} \mathcal{P}_{ii} &= \mathcal{P}_{ii}^{0} \odot \mathcal{Q}_{ii} \odot \mathcal{P}_{ii}^{0} \\ &= \cup_{p=1}^{\infty} (\mathcal{P}_{ii}^{0} \odot \hat{\mathcal{Q}}_{ii}^{1})^{p} \odot \mathcal{P}_{ii}^{0}. \end{aligned} \tag{6}$$

Let us define the contributions,

$$\begin{aligned} \kappa(\hat{\mathcal{Q}}_{ii}^{1}) &= \Sigma_i \\ \kappa(\mathcal{P}_{ii}^{0}) &= g. \end{aligned} \tag{7}$$

Then from equation (6) taking contributions of either side we immediately obtain

$$\kappa(\mathcal{P}_{ii}) = \sum_{p=1}^{\infty} (g\Sigma_i)^p g.$$

If we put this back into the expression of the Feenberg series we obtain

$$\begin{aligned} G_{ii}(z) &= g + g\Sigma_i g + g\Sigma_i g \Sigma_i g + \cdots \\ &= g + g\Sigma_i G_{ii}(z). \end{aligned}$$

This is the *Dyson equation*. Since g is totally diagonal, it follows that,

$$G_{ii} = \frac{1}{z - \epsilon_i - \Sigma_i(z)} \tag{8}$$

where $\Sigma_i(z)$ is called the *self-energy*. The effect of the multiple scattering is to *renormalize* the unscattered Hamiltonian $\boldsymbol{H}_0$ to an *effective* Hamiltonian $\boldsymbol{H}_{\text{eff}} = \Sigma_i(\epsilon_i + \Sigma_i)|i\rangle\langle i|$. This effective Hamiltonian is not self-adjoint but nevertheless has exactly the same spectrum as the full Hamiltonian $\boldsymbol{H}$.

A very simple example illustrates the effect of this self energy. If $\boldsymbol{H}_0$ denotes the Hamiltonian of a set on non-interacting atoms. The energy of the ith electron is given by ϵ_i. When the interaction $\boldsymbol{H}_1$ between the atoms is turned on, that is, when these atoms bond to form the solid, the real part of the self-energy leads to a shift in the energy levels of the electrons because of the bonding. The imaginary part leads to a broadening of the sharp energy levels to form bands.

In the case $\boldsymbol{H}_0$ is totally diagonal, the multiple scattering decorates only vertices. However, if $\boldsymbol{H}_0$ has links as well, then the multiple scattering decorates both vertices and links.

2.4. Renormalization of the multiple-scattering series

In this section we shall study the self-energy decoration and obtain a modified or renormalized expression for its contribution. Let us look back at figure 2. Note that the closed loose ended path S_{ii}^N, into which paths $Q_{ii}^{p,N}$ were broken up, do not visit the vertex v_i at all, but they may visit other vertices v_j more than once. Let us start regrouping paths again. In figure 1 the path labelled $N = 4$, $p = 1$ in the top row of the third column, visits the next vertex v_{i_1} twice. So do the paths labelled $N = 5$, $p = 1$ in the second column of the second row and $N = 6$, $p = 1$ in the first column of the last row. Let us group together such paths which visit the vertex v_{i_1} once, twice and so on. This is shown in figure 3.

Now, the loose ended closed paths that decorate the vertex v_{i_1} are all paths of all lengths which start and end at v_{i_1}, but never visit the vertex v_1. This decoration may be written as

$$\mathcal{P}^0_{v_{i_1},v_{i_1}} + \mathcal{P}^0_{v_{i_1},v_{i_1}} \odot \mathcal{Q}^{(v_i)}_{v_{i_1},v_{i_1}} \odot \mathcal{P}^0_{v_{i_1},v_{i_1}} = \mathcal{P}^{(v_i)}_{v_{i_1},v_{i_1}}.$$

The expression $\mathcal{Q}^{(v_i)}_{v_{i_1},v_{i_1}}$ is exactly similar to $\mathcal{Q}_{ii}$ of equation (5), the only difference is that the superscripted vertex is never visited. So that paths are counted on a network from which the superscripted vertex has been removed. Exactly as in equation (5) this set of paths can be broken up into a set of paths that visit the vertex v_{i_1} only once (that is at the beginning and end, but never inside):

$$\mathcal{Q}^{(v_1)}_{v_{i_1},v_{i_1}} = \cup_{p=1}^{\infty} \hat{\mathcal{Q}}^{1,(v_i)}_{v_{i_1},v_{i_1}} \odot (P^0_{v_{i_1},v_{i_1}} \odot \hat{\mathcal{Q}}^{1(v_1)}_{v_{i_1},v_{i_1}})^{p-1}.$$

Once we compare the above two equations, it becomes clear that the contribution of the decoration is,

$$\kappa(\mathcal{P}^{(v_1)}_{v_{i_1},v_{i_1}}) = G^{(i)}_{i_1 i_1}. \tag{9}$$

Thus the effect of the regrouping is to renormalize the contribution of the vertex v_{i_1} from $\kappa_(v_{1_i}) = g_{i_1 i_1}$ to $\hat{\kappa}(v_{i_1 i_1}) = G^{(i)}_{i_1 i_1}$.

We go on to the next vertex in line v_{i_2} and again regroup paths in exactly the same way. The effect of this regrouping will be to renormalize the contribution of the vertex to $G^{(i,i_1)}_{i_2 i_2}$. As before, the superscripted vertices denote that the Green function is calculated from the network in which the superscripted vertices are removed, so that no path can ever visit them.

We now systematically go on regrouping vertex by vertex until all vertices are exhausted. The final results may be summarized as follows.

(1) Since in the regrouping procedure we have taken into account paths of all lengths which visit every vertex as many times as possible, we have, in effect, taken care of all possible paths on the network.

(2) After renormalization, the remaining paths never visit any of the internal vertices more than once. Such paths are called *self-avoiding paths*.

(3) The contribution of a vertex on a path is now entirely dependant on the path, since it depends on all the preceding vertices. If we have a self-avoiding path $\{v_1, \ell_{12}, v_2, \ldots, v_r, \ell_{rr+1}, v_{r+1} \ldots\}$, then the renormalized contribution of the rth vertex is $\hat{\kappa}(v_r) = G_{r,r}^{(1,2,\ldots,r-1)}$.

(4) Every intermediate Green function

$$G_{rr}^{(1,2,\ldots,r-1)} = (z - \epsilon_r - \Sigma_r^{(1,2,\ldots,r-1)})^{-1}$$

and the self-energies may be obtained by the same path contribution expression as (7) except that the superscripted vertices are removed from the network while the calculation proceeds.

$$\hat{\kappa}(\hat{\mathcal{Q}}_{rr}^{(1,2,\ldots,r-1)}) = \Sigma_r^{(1,2,\ldots,r-1)}.$$

This result with the modified definition of the contribution of vertices and the self-energy in terms of self-avoiding paths is the *renormalized Feenberg series*.

$$G_{ii}(z) = \hat{\kappa}(\mathcal{P}_{ii}^0) + \hat{\kappa}(\mathcal{P}_{ii}).$$

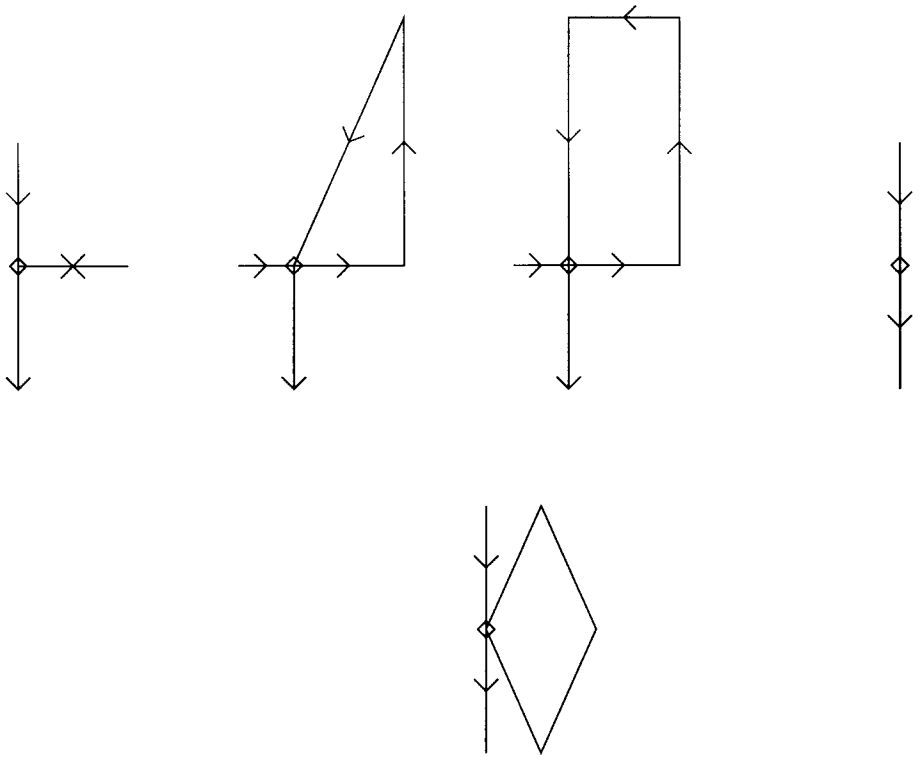

Figure 3. Grouping of the paths to illustrate decorations of internal vertices.

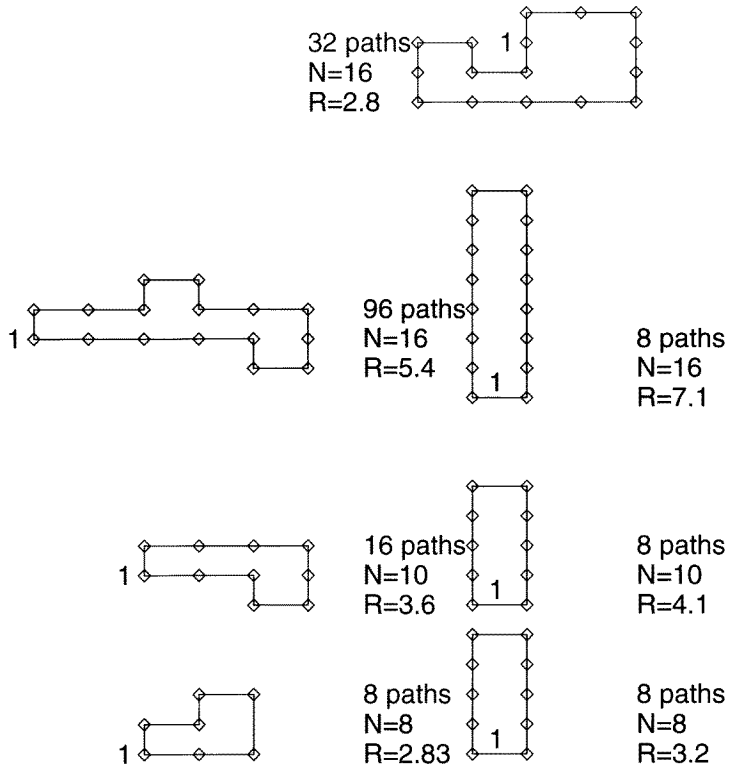

Figure 4. Closed paths labelled by their lengths N and their range R, as well as the number of such paths possible on the square lattice. This illustrates that as N increases such paths are dominated by those that wind round the starting vertex labelled by 1.

3. Applications of the geometric formulation

The geometric formulation put forward in the previous sections is mathematically appealing, but the question always arises: does this geometric formulation have any applications to problems of physics? We shall now discuss areas where the pathcounting procedure has been utilized to give insight into the solution of the problem and interpretation of its results. As mentioned earlier, such applications become important when the Hamiltonian is either spatially or topologically random and the usual band-structure methods available for translationally symmetric crystalline lattices become inapplicable. The path-counting technique then allows us to set up physically appropriate approximations.

The exact Green function of any Hermitian Hamiltonian with a bounded spectrum of any system, with or without disorder, must satisfy the so-called Herglotz analytic conditions. A complex function $f(z)$ of a complex variable z is called Herglotz if (i) the singularities of the function lie entirely on the real z-axis, (ii) the sign of the imaginary part of $f(z)$ is always negative in the upper half of the complex z-plane and always positive in the lower half and (iii) the real part of $f(z)$ varies as $1/z$ as $z \to \infty$ along the real z-axis. Physical constraint of a real spectrum, a non-negative density of states and a bounded spectrum necessitates these conditions. Any approximation therefore must also be such that the approximate Green function also obeys these conditions. Haydock [1] has shown earlier that any path contribution of the type discussed earlier satisfies these analytic conditions. Therefore, any

approximation which is based on considering only a specific class of paths maintains the Herglotz properties. We shall consider two specific examples of such applications.

3.1. Evolution of density of states structures related to paths

An example of a much more direct application of the graphical formalism occurs if we wish to relate the structure in the density of states to specific paths on the lattice. The number and shape of paths on the lattice is a property of the topology of the lattice. So, what we wish to study here is the effect of the lattice topology on the shape and structures in the density of states. In the case in which the lattice becomes topologically distorted and paths of new shapes occur, the following discussion will allow us to choose the dominant distorted paths to include in our approximation.

As an example let us take the square lattice, on which we define a tight-binding Hamiltonian with one orbital per site

$$H_{ij} = \sum_i \sum_{j \epsilon N_1} t_{ij}.$$

The equal diagonal elements taken to be zero by this choice of the energy origin and N_i are the nearest neighbours of the vertex v_i on the square lattice. These off-diagonal elements can be chosen to be 1 with this choice of the energy scale.

The simplest approximation to the square lattice is the Cayley tree, shown in the top row of figure 5. Both have the same number of nearest neighbours per site. What the Cayley tree lacks as compared with the square lattice are closed self-avoiding loops starting from a site and back. If we begin by neglecting the contribution of these self-avoiding loops, the path contribution gives the following: (see the top row, second column of figure 5). Since there are only four self-avoiding paths from the vertex 1 and back and all of these are of length 2,

$$\begin{aligned} G_{11} &= (z - \Sigma_1)^{-1} \\ \Sigma_1 &= \sum_{k=1}^{4} \kappa(P_k^2) \\ &= 4G_{22}^{(1)}. \end{aligned}$$

The graph with the central site labelled 1 removed is shown on the extreme right in the top row of figure 5. There are now only three closed, self-avoiding paths from 2 and back and all are identical of length 2. At this stage we note that the graph with the vertex 1 removed and that with $(1, 2)$ removed are identical (this is a specific feature of the Cayley tree, which has no closed loops at all). This gives,

$$\begin{aligned} G_{22}^{(1)} &= \Gamma \\ &= (z - \Sigma)^{-1} \\ \Sigma &= 3\Gamma. \end{aligned}$$

The above set of equations is closed and may be solved directly:

$$G_{11}(E) = \begin{cases} \left(E - 2\mathrm{i}\sqrt{12 - E^2}\right)/(16 - E^2) & \text{if } -\sqrt{12} \leqslant E\sqrt{12} \\ 3/\left(E - 2\sqrt{E^2 - 12}\right) & \text{if } |E| \geqslant 12. \end{cases}$$

The density of states is featureless and symmetric. The band width is around 7.32 instead of 8 as predicted from Bloch theorem based band structure. There is a signature

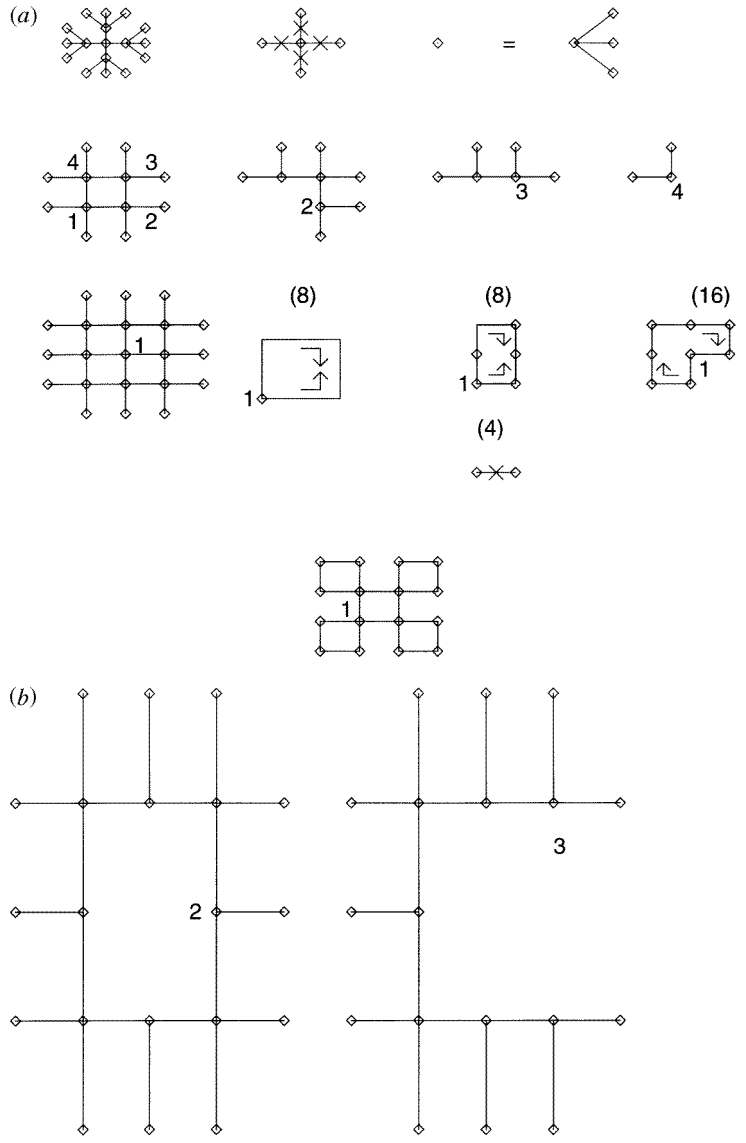

Figure 5. (*a*) Showing different approximations to the square lattice.(top) The Cayley tree, the four closed paths from the origin and back and the peripheral decorations. (second) A single square immersed in the Cayley tree and break-up of the square path by successively removing vertices on the path. (third) A small square lattice immersed in the Cayley tree and the different closed loops included. (bottom) A Husimi cactus. (*b*) Break-up of the closed loops shown in the third row of figure 5 by successively removing vertices on the path.

of neither the logarithmic van Hove singularity at the origin nor the two flanking kink singularities which are characteristic of the density of states on square lattices. This is shown in figure 6(i).

Note that in figures 6–8 the x-axes plot the energy scaled by the band width, the left-hand edge chosen as the zero of energy. The density of states shown here are thus non-zero in the range $0 \leqslant E \leqslant 1$. The y-axes show the density of the states, again scaled by its

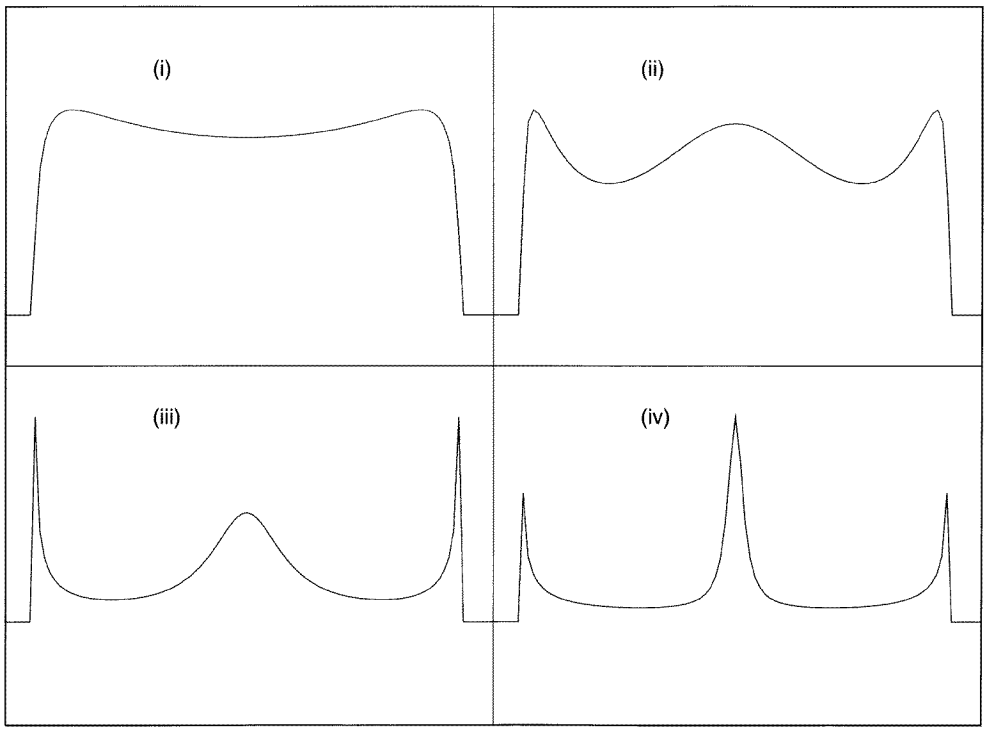

Figure 6. The density of states (states/atom-energy) where the energy is scaled by the band width. (i) For the Cayley tree, (ii) for the single square immersed in the Cayley tree, (iii) for the square piece immersed in the Cayley tree and (iv) for the Husimi cactus.

maximum value. Since we are primarily interested in the shape of the density of states and structures in it related to the topology of the lattice, the scaled axes suffice. In more realistic calculations the x-axes should be given in (say) Ryd and the y-axes in states/atom-Ryd-spin.

The next smallest closed loop is the square shaped loop shown in the second row in figure 5. Let us consider only one such loop and the contributions of all other closed loops in the lattice are ignored. This means that the contribution of the decorations on the vertices in the periphery are those of the Cayley tree. Now we still have four self-avoiding paths of length 2 starting from 1 and back but, in addition, there are two closed loops of length 4. These are the paths along the central square loop clockwise and anti-clockwise from 1 and back. The second row of the second column shows that the graph with the vertex 1 omitted resembles the old Cayley tree with the starting site removed, except that the site 4 along the loop has one less link than in the tree (the link that was associated with the removed vertex).

The contribution of the closed loop to the self-energy is

$$\Sigma^{(4)} = G_{22}^{(1)} G_{33}^{(1,2)} G_{44}^{(1,2,3)}.$$

Looking at the figure in the second column of the second row of figure 5 we obtain

$$G_{22}^{(1)} = \boldsymbol{K}_{n=1}^{3} \frac{1}{z - 2\Gamma -}$$

$$G_{33}^{(1,2)} = \boldsymbol{K}_{n=1}^{2} \frac{1}{z - 2\Gamma -}$$

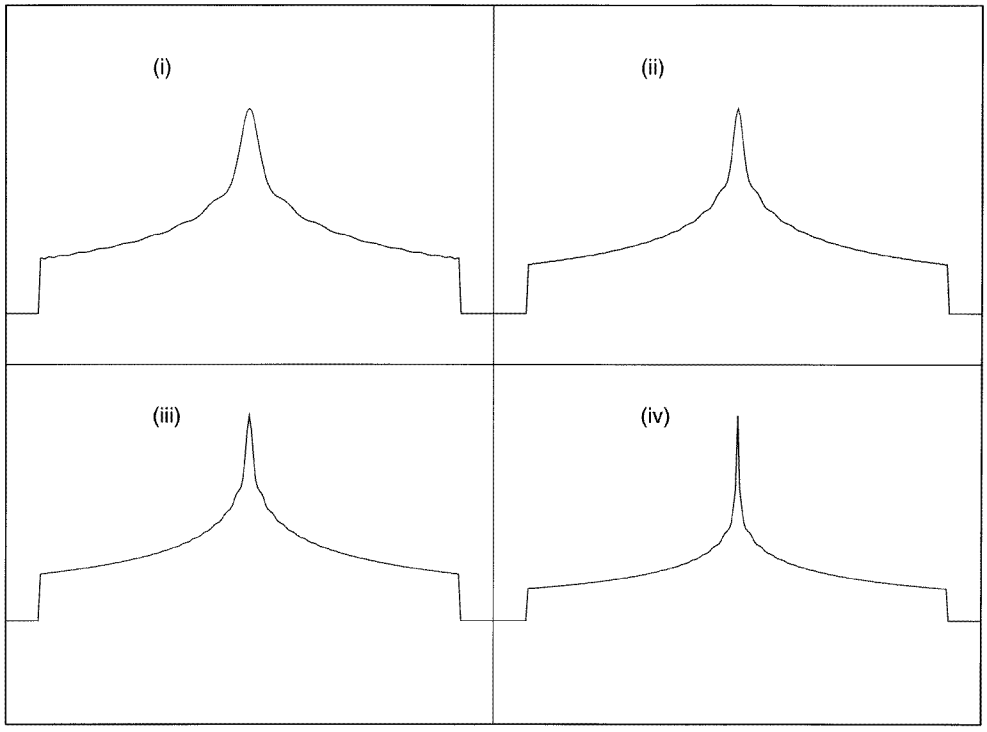

Figure 7. The density of states (states/atom-energy) where the energy is scaled by the band width. These were obtained by the recursion on a square lattice. For (i) 20 (ii) 40 (iii) 60 and (iv) 200 recursions.

$$G_{44}^{(1,2,3)} = \frac{1}{2\Gamma}.$$

The equations again form a closed set and we may solve for the various contributions. We finally obtain

$$G_{11} = \frac{1}{z - 2\Gamma - 2\Sigma^{(4)}}.$$

The density of states is shown in figure 6(ii). Already with the inclusion of only one square loop the incipient logarithmic van Hove singularity at the origin begins to show up. So do singularities at the flanks of the density of states.

In our next stage of approximation we include a central patch of square lattice immersed in a Cayley tree. This is shown in the first column of the third row in figure 5. We now have to count all the self-avoiding paths from vertex 1 and back. from this figure we can identify four classes: four walks of length $2P_{11}^2$, eight square loops (clockwise and anticlockwise) P_{11}^4; 16 rectangular loops P_{11}^6 (clockwise and anticlockwise with both x- and y-elongations) and 16 L-shaped loops P_{11}^8. All these walks are shown in the third row of figure 5 with their weights.

The calculations of the self-energy also requires $G_{22}^{(1)}$ and $G_{33}^{(1,2)}$. The graphs for these calculations are shown in the inset.

The self-energy for $G_{22}^{(1)}$ has contributions from one path P_{22}^2, shown going towards the right with a Cayley tree decorating its extremity. Its contribution is Γ. There are two other paths of length 2: those going above and below vertex 2. Contribution of these

(*a*)

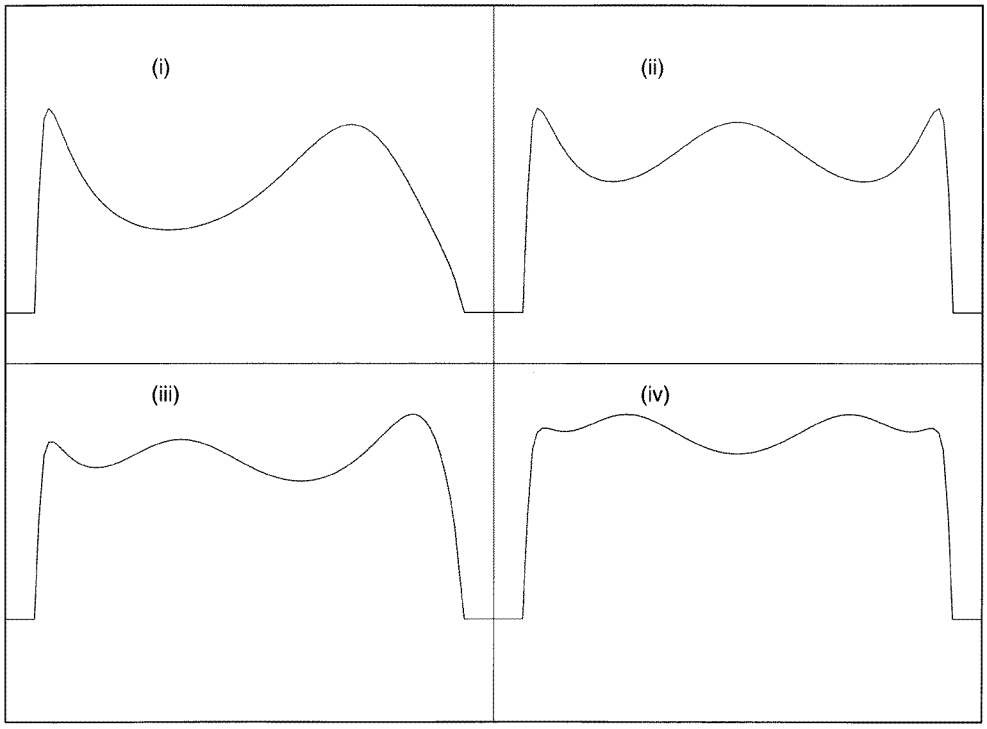

(*b*)

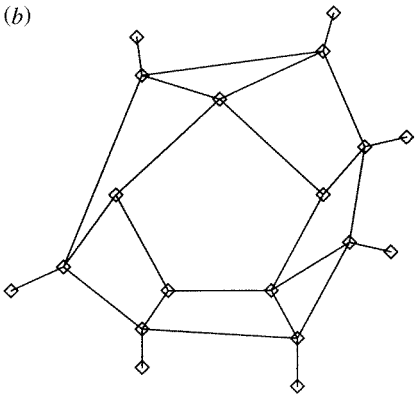

Figure 8. (*a*) The density of states (states/atom-energy) where the energy is scaled by the band width. These are for (i) three- (iv) four- (iii) five- and (iv) six-membered rings immersed in the Cayley tree. (*b*) A distorted network showing distorted squares as well as triangular and pentagonal rings. (*c*) The density of states (states/atom-energy) where the energy is scaled by the band width. The full curve was calculated for a network with 62% square, 25% triangular and 13% pentagonal rings immersed in the Cayley tree. For comparison we show the density of states of the peice of square lattice immersed in the Cayley tree shown earlier (broken curve).

together gives $2G_{33}^{(1,2)}$. These are also two square paths of length 8 whose contribution is $2G_{33}^{(1,2)}G_{44}^{(1,2,3)}\ldots G_{99}^{(1,2,\ldots,8)}$.

The graph for $G_{33}^{(1,2)}$ and the other subsequent Green functions all resemble the Cayley

(*c*)

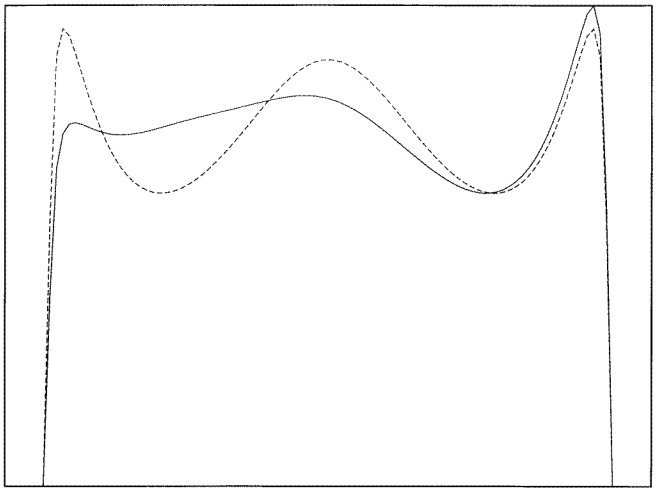

Figure 8. (Continued)

tree. The main one is shown in the inset to the right. The only difference is that the decorations on alternate vertices are different in number to the full Cayley tree. This arises because of the connection of these vertices to vertex 1 which has been removed.

Again this set forms a closed set of equations which can be solved. The resulting density of states is shown in figure 6(iii). We note that the inclusion of a bigger chunk of square lattice topology in the neighbourhood of the starting point has lead to a sharpening of the van Hove singularities both at the centre and at the flanks of the density of states. These structures seem therefore to be intrinsically related to the topology of the lattice and not to the magnitude of the Hamiltonian matrix elements.

As a final illustration, we show the results of a Husimi cactus lattice. This lattice is shown in the bottom row of figure 5. The Husimi cactus is a generalization of case (ii), where the central square loop instead being decorated with Cayley trees at its extremities, are decorated by other square loops. We thus take square-loop contributions infinitely far into the lattice. However, the loops don't intersect, so that the outward topology of the lattice is approximated. Again the equations for the self-energy forms a closed set of equations which can be obtained by looking at the contributions of the various paths shown in figure 5 bottom row.

The resulting density of states,

$$G_{11} = (z - 2\Sigma)^{-1}$$
$$\Sigma = 2G_{22}^{(1)} + 2G_{22}^{(1)}G_{33}^{(1,2)}G_{44}^{(1,2,3)}$$
$$G_{22}^{(1)} = (z - \Sigma - G_{33}^{(1,2)})^{-1}$$
$$G_{33}^{(1,2)} = (z - \Sigma - G_{44}^{(1,2,3)})^{-1}$$
$$G_{44}^{(1,2,3)} = (z - \Sigma)^{-1}.$$

The resulting density of states is shown in figure 6(iv). Note that the logarithmic van Hove singularity at the band centre is now almost evident from the figure, confirming that this structure is related to the square-loop topology of the lattice.

We may now compare these densities with more accurate results obtained from the

recursion method [3, 4]. These are shown in figures 7(i)–(iv). The termination of recursion in (i)–(iv) is carried out after 20, 40, 60, and 400 steps. In the last calculation we have reduced the rank of the space on which the recursion is carried out using the point-group symmetries of the square lattice [5]. The growth of the central logarithmic van Hove singularity with the inclusion of longer paths in the recursion shows up clearly, confirming our results from simple path-contribution considerations. The singularities on the two flanks of the density of states appear to be of a different kind, though. In the recursion (and exact Bloch theorem considerations) the singularities appear as discontinuities in the derivative. However, in the tree or cacti type of approximations these appear as integrable divergences. The exact nature of these singularities therefore depend sensitively not on square loops alone, but on the asymptotic topology of the lattice.

3.2. Examples on random networks

The example in the previous section was described in detail to show how fairly simple considerations of the path-contribution idea developed in this communication can give us extensive insight into the structures in the density of states. These are otherwise obtained from very expensive computer calculations. The above discussion also leads the way for us to model more complex situations, for example, calculations on random networks. If we begin to randomly distort the perfectly square lattice of the previous example, but at the same time make sure that the network still spans the space, we shall end up with the kind of situation shown in figure 8(*b*). The shape of the network is usually relaxed to minimize energy. Such continuous random networks have been cited in literature. Two new features show up in the network. First, apart from the usual square loops we now have a proportion of three- and five-membered loops as well. Second, although most sites are still four-fold coordinated, a small proportion of sites miss a bond (e.g. three sites of the pentagonal ring in figure 8(*b*)). These are the dangling bonds which give rise to localized states often in the energy gaps.

The path-contribution method is then an ideal way of studying the effect of different topologically distorted loops on the density of states. The procedure we follow is similar to the previous section. The topology of the network in the immediate vicinity of the site to be examined is considered as exactly as possible, while the far away part of the network is approximated by tree or cacti containing at least the most important loops which contribute to the structures in the density of states. We shall not repeat details of the mathematics, but illustrate some of the results.

In figure 8(*a*) we show the local density-of-states structures which arise from three, four, five and six-membered loops. The characteristic incipient van Hove singularity of the square loops (shown in (ii)) is destroyed by the presence of odd-membered loops. These new topological structures have a considerable effect on the spectral distribution and hence on specific physical properties of the network. In figure 8(*c*) we show the total density of states for the network shown in figure 8(*b*) in which roughly 62% of the loops are square, but about 25% are triangular and 13% are pentagonal. We have modelled such a network with a central random network immersed in a tree background. This is similar to the central square network immersed in a tree background. The total density of states is compared in the two cases. As mentioned before, van Hove singularity structures within the band are broadened out and there is considerable redistribution of spectral weight within the band.

As the paths considered becomes longer and longer, the book-keeping of self-avoiding paths become rapidly intractable. Although a brute-force numerical solution is an alternative method, in trying to understand the data produced and analysing the effect of topology on

the electronic spectra, it is always instructive to use the path-contribution technique to gain insight first before reaching conclusions about numerical results. It is here that the method proposed in this communication has importance.

4. Conclusion

We have given here a graphical reinterpretation of the renormalizing Feenberg perturbation series. The path-counting technique brings out some of the earlier results in a transparent form. This path-counting technique provides a powerful insight into how to generate physically relevant approximations in situations where the underlying lattice is topologically distorted and the usual band-structure methods on translationally symmetric lattices become inapplicable. Similarly, in case of substitutional disorder, this technique in tandem with augmented-space method, has been used earlier to generate analytic generalizations of the single-site mean-field coherent potential approximations [6]. In such situations the path-counting interpretation discussed here provides an invaluable technique.

Acknowledgments

ND would like to thank the Council for Scientific and Industrial Research, Government of India for financial assistance.

References

[1] Haydock R 1972 *PhD Thesis* University of Cambridge, Cambridge
Haydock R 1974 *J. Phys. A: Math. Gen.* **7** 2120
[2] Bishop A R and Mookerjee A 1974 *J. Phys. C: Solid State Phys.* **7** 2145
Kumar V, Mookerjee A and Srivastava V K 1982 *J. Phys. C: Solid State Phys.* **15** 1939
[3] Haydock R, Heine V and Kelly M J 1975 *J. Phys. C: Solid State Phys.* **8** 2591
[4] Haydock R 1980 *Solid State Physics* vol 35 (London: Academic) p 246
[5] Saha T, Dasgupta I and Mookerjee A 1996 *J. Phys.: Condens. Matter* **6** L245
[6] Mookerjee A 1992 *Electronic Structures of Metals and Alloys* ed O K Anderson, V Kumar and A Mookerjee (Singapore: World Scientific)